Practical Modeling of Metal Hydride Hydrogen Storage Systems

Sarang A. Gadre, Armin D. Ebner, Shaheen A. Al-Muhtaseb, and James A. Ritter*

Department of Chemical Engineering, Swearingen Engineering Center, University of South Carolina, Columbia, South Carolina 29208

A new approach is introduced to model the discharge behavior of a metal hydride hydrogen storage bed. The reversible reaction kinetics and the empirical van't Hoff relationship used in a typical reactor model are replaced by a solid-phase diffusion equation and a semiempirical equilibrium $P-C-T$ relationship. Two new semiempirical $P-C-T$ models are also introduced based on modified virial and composite Langmuir expressions. By varying the heat- and mass-transfer coefficients, the model was calibrated to experimental pressure and temperature histories obtained from a commercially viable metal hydride bed containing $Lm_{1.06}Ni_{4.96}Al_{0.04}$. Overall, the results of this study showed that a fairly simple numerical model can do a reasonable job in predicting the discharge behavior of a fairly complicated metal hydride hydrogen storage bed over a wide range of hydrogen flow-rate demands. The extreme theoretical limits of isothermal equilibrium (analytical model), adiabatic equilibrium, nonadiabatic equilibrium, isothermal nonequilibrium, and adiabatic nonequilibrium conditions were also studied and compared to the actual behavior under nonadiabatic nonequilibrium conditions. These limiting cases revealed that the metal hydride hydrogen storage vessel was definitely heat-transfer-limited and only minimally mass-transfer-limited over a wide range of hydrogen discharge flow rates.

Introduction

Hydrogen as an energy source is receiving increasing attention around the world because the demand for environmentally cleaner fuels is on the rise. Its use, however, necessitates the development of a hydrogen refueling and storage infrastructure, with safety being a major concern. Consequently, metal hydrides, as a hydrogen storage medium, have been under consideration for many years[1,3−17] because they have the ability to store H_2 reversibly in the solid state at relatively low pressures and ambient temperatures. The utility of metal hydrides as a hydrogen storage medium was demonstrated recently by the Savannah River Technology Center (SRTC). They developed an on-board hydrogen storage system for a hybrid electric bus,[1] based on the commercially viable $Lm_{1.06}Ni_{4.96}Al_{0.04}$ metal hydride (Lm = La 55.7, Ce 2.5, Pr 7.7, and Nd 34.1 atomic %).

This system consists of a bank of horizontal tubes partially filled with metal hydride interdispersed within a highly porous aluminum foam matrix for heat transfer. Each column contains a horizontal porous metal filter feed tube and a U-tube, single-pass heat exchanger for additional heat transfer via an aqueous medium. These intricacies of the SRTC hydrogen storage system are shown in Figure 1.[1,3−5] Clearly, this metal hydride hydrogen storage system is quite challenging to describe mathematically; nevertheless, a mathematical description is highly desirable for design, development, and optimization. Therefore, the objective of this paper is to introduce a new approach for modeling metal hydride H_2 storage systems from a very practical point of view.

H_2 is stored in a metal hydride by a process called hydrogenation, and it is withdrawn from the material by a process called dehydrogenation. This charge/discharge process is quite complicated because of the inherent heat- and mass-transfer/reaction phenomena associated with it. Most of the mathematical models presented in the literature that describe these dynamic phenomena, in addition to the mass and energy balances, necessarily make use of reactor design equations that include a reaction kinetics equation. The reason for this approach is that this process can be classified as a reversible chemical reaction. However, because the reaction rate tends to be very fast, the charge/discharge process from a metal hydride bed can also be modeled as a heat-transfer-limited, solid-state, diffusion-controlled process with the equilibrium relationship described by a reversible pressure−composition−temperature ($P-C-T$) diagram. Thus, in this new approach, the reversible reaction kinetics and the empirical van't Hoff relationship used in a typical reactor model (that includes mass and energy balances) are replaced by a solid-phase diffusion equation and a semiempirical equilibrium $P-C-T$ relationship.

The first part of this paper introduces two new adsorption isotherm relationships that describe the S-shaped characteristics of the $P-C$ diagram as a function of temperature. Then a very simple dynamic model of the H_2 discharge process is introduced, which, under isothermal and equilibrium conditions, represents an upper thermodynamic limit for the process performance. This model can be used to rapidly determine the feasibility of a metal hydride material for H_2 storage. A more complex and hence more realistic model of the H_2 discharge process is introduced next. This model, by accounting for heat- and mass-transfer resistances, represents a more realistic picture of the process performance; therefore, it can be used for process design and development.

These models are compared to experimental discharge curves obtained from one of the SRTC metal hydride hydrogen storage columns, identical with that used in

* To whom correspondence should be addressed. Phone: (803) 777-3590. Fax: (803) 777-8265. E-mail: ritter@engr.sc.edu.

10.1021/ie020839i CCC: $25.00
Published on Web 03/20/2003

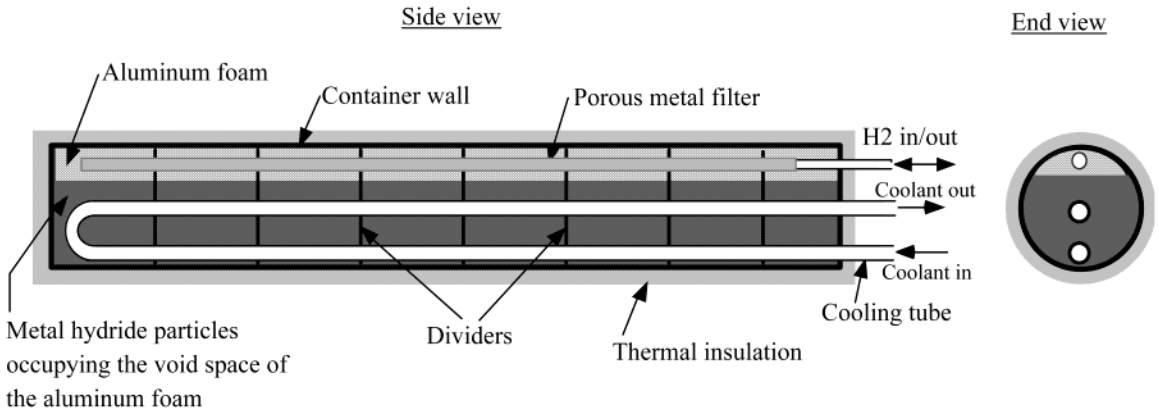

Figure 1. Schematic of the SRTC metal hydride hydrogen storage vessel.[1,3−5]

the hybrid bus demonstration project.[1] The heat- and mass-transfer coefficients associated with the SRTC system are also obtained by comparing the theoretical discharge curves with the experimental ones. The extreme theoretical limits of isothermal equilibrium, adiabatic equilibrium, nonadiabatic equilibrium, isothermal nonequilibrium, and adiabatic nonequilibrium conditions are also explored to gain an appreciation for the limiting and actual behaviors of the SRTC system.

Theoretical Section

Modified Virial (MV) Isotherm Model. A MV adsorption isotherm of the form

$$\ln(\phi^*\pi) = \left(A_0 + \frac{A_1}{\theta}\right) + \left(B_0 + \frac{B_1}{\theta}\right)\frac{1}{\phi^*} + C_0\phi^{*k} \quad \text{for } \phi^* \geq \phi_H \text{ and } \phi^* \leq \phi_L \quad (1)$$

can be used to describe the $P-C$ relationship outside the tie line (phase-change envelope). The tie-line envelope can be described empirically by

$$\phi_H = \left(a_H + \frac{b_H}{\theta^2}\right)^{1/2} \quad (2)$$

$$\phi_L = \left(a_L + \frac{b_L}{\theta^2}\right)^2 \quad (3)$$

where the isotherm relationship inside the envelope is obtained by linear interpolation between ϕ_H and ϕ_L as

$$\frac{\phi^* - \phi_L}{\pi - \pi_L} = \frac{\phi_H - \phi_L}{\pi_H - \pi_L} \quad (4)$$

An expression for the heat of adsorption is obtained by applying eq 1 to the Clausius−Clapeyron equation for adsorption.[18] The resulting simple loading-dependent expression is given by

$$\Delta H = RT_0\left(A_1 + \frac{B_1}{\phi}\right) \quad (5)$$

Composite Langmuir (CL) Isotherm Model. A typical isothermal $P-C$ curve exhibiting a phase change resembles two Langmuir isotherms connected at a so-called switch point. One of the equations describes the $P-C$ behavior up to the phase change, and the other describes the phase change behavior and beyond as pressure increases. It is a simple matter to combine two Langmuir isotherms in this way[19] and obtain the following CL isotherm:

$$\phi^* = \begin{cases} \dfrac{\phi_S(1 + b_1 {P_0}^{0.5}{\pi_S}^{0.5})\pi^{0.5}}{(1 + b_1 {P_0}^{0.5}\pi^{0.5}){\pi_S}^{0.5}}, \quad b_1 = b_{10}\exp\left(-\dfrac{\Delta H_1}{RT}\right) & \pi \leq \pi_S \\ \phi_S + \dfrac{(\phi_{max} - \phi_S) b_2 {P_0}^{0.5}(\pi^{0.5} - {\pi_S}^{0.5})}{1 + b_2 {P_0}^{0.5}(\pi^{0.5} - {\pi_S}^{0.5})}, \quad b_2 = b_{20}\exp\left(-\dfrac{\Delta H_2}{RT}\right) & \pi \geq \pi_S \end{cases} \quad (6)$$

with the square-root pressure dependence accounting for the dissociation of molecular hydrogen to atomic hydrogen.[20] π_S and ϕ_S are the switch pressure and loading that correspond to the point on the isotherm where the phase transition starts (i.e., the bottom border of the envelope). These switch variables are related to θ according to

$$\ln(\pi_S P_0) = d_0 + \frac{\Delta H_S}{RT_0\theta} \quad (7)$$

where ϕ_S is the loading at the switch condition and ΔH_S is the heat of adsorption corresponding to the bottom end of the phase transition envelope. The loading- and temperature-dependent heat of adsorption is given by

$$\Delta H = \begin{cases} 2\Delta H_1 = \Delta H_S & \pi \leq \pi_S \\ 2[\Delta H_2 + (\dfrac{\Delta H_S}{2} - \Delta H_2)\dfrac{{\pi_S}^{0.5}}{\pi^{0.5}}] & \pi > \pi_S \end{cases} \quad (8)$$

Bed Porosities. As explained earlier, the complex SRTC bed is completely filled with porous aluminum foam, the voids of which are only partially filled with metal hydride particles to provide space for expansion during hydrogenation. In the development of the mathematical models, it is assumed that the entire bed is filled with aluminum foam with void fraction ϵ_{Al}. It is further assumed that the metal hydride particles, with packing void fraction ϵ_{mH}, occupy only some specified fraction f_r of the empty volume (ϵ_{Al}) within the pores of the aluminum foam. For this particular system, because the masses and densities of aluminum and

metal hydride particles are known, the following expressions are easily derived:

$$\epsilon_1 = 1 - \frac{m_{mH}/\rho_{mH}}{\pi(r_o^2 - r_i^2)L} = 1 - \epsilon_{Al} f_r (1 - \epsilon_{mH}) \quad (9)$$

$$\epsilon_2 = 1 - \frac{m_{mH}/\rho_{mH} + m_{Al}/\rho_{Al}}{\pi(r_o^2 - r_i^2)L} = (1 - f_r)\epsilon_{Al} + f_r \epsilon_{Al} \epsilon_{mH} \quad (10)$$

where ϵ_1 represents the fraction of the bed volume not occupied by the metal hydride particles; thus, $1 - \epsilon_1$ represents the fraction of the bed occupied solely by the metal hydride particles. Similarly, ϵ_2 represents the fraction of the bed not occupied by either the metal hydride particles or the aluminum foam; i.e., ϵ_2 represents the total void fraction in the bed. The expressions on the right-hand side of eqs 9 and 10 can be used if the masses and densities of the aluminum foam and metal hydride particles are not known, which is more typical. In fact, they are more amenable for scaling and design studies because they only depend on the porosities, ϵ_{Al} and ϵ_{mH}, and the specified fraction f_r.

Analytical Charge/Discharge Model. The analytical model (AM) for discharge is based on the following assumptions: The H_2 discharge process, starting from a fully charged state at constant temperature and pressure, is carried out isothermally, with no mass- or heat-transfer resistances. The H_2 discharge flow rate is so slow that axial pressure gradients are negligible and ideal plug flow is assumed. The gas is also assumed to be ideal. Based on these assumptions, the one-dimensional (1-D) mass balance in a packed metal hydride bed is given by

$$\epsilon_2 \frac{\partial c}{\partial t} + \epsilon_2 \frac{\partial (vc)}{\partial z} + \frac{\rho_{mH}}{M_{H_2}}(1 - \epsilon_1)\frac{\partial q}{\partial t} = 0 \quad (11)$$

By substituting $c = P/RT$ and assuming instantaneous equilibrium,

$$\epsilon_2 \frac{1}{RT}\frac{\partial P}{\partial t} + \epsilon_2 \frac{P}{RT}\frac{\partial v}{\partial z} + \frac{\rho_{mH}}{M_{H_2}}(1 - \epsilon_1)\frac{\partial q}{\partial t} = 0 \quad (12)$$

Also, by assuming a linear velocity profile, $v(z) = k'z$, one end closed, $v(0) = 0$, and a constant outlet velocity, $v(L) = v_{out}$,

$$\frac{\partial v}{\partial z} = k' = \frac{v_{out}}{L} \quad (13)$$

As the pressure decreases during discharge, the outlet velocity changes. If the molar flow rate (and, hence, flux f) exiting the column is predefined as a constant value, the variation of the outlet velocity with pressure can be written as

$$\frac{\partial v}{\partial z} = \frac{k}{P} \quad (14)$$

where $k = fRT/L\epsilon_2$. Substituting eq 14 into eq 11 results in the following ordinary differential equation:

$$\epsilon_2 \frac{1}{RT}\frac{dP}{dt} + \frac{f}{L} + \frac{\rho_{mH}}{M_{H_2}}(1 - \epsilon_1)\frac{dq}{dt} = 0 \quad (15)$$

Integrating eq 12 with initial conditions: at $t = 0$, $P = P_i$, and $q = q_i$ yields

$$t = \frac{L\epsilon_2}{f}\left[\frac{(P_i - P)}{RT} + \frac{\rho_{mH}(1 - \epsilon_1)}{M_{H_2}\epsilon_2}(q_i - q)\right] \quad (16)$$

which describes the discharge time as $f(P)$ in terms of the metal hydride properties (ρ_S and $P-C-T$), the bed length (L), and the molar flux (f), which also specifies the column diameter. Any adsorption isotherm relationship, like the MV and CL models, can be used to obtain the expression for q as a function of P (as well as q_0, corresponding to P_0). It is also a simple matter to convert this model into one that describes the charge process by simply changing the initial conditions and following an increase in pressure instead of a decrease.

Numerical Charge/Discharge Model. The numerical model (NM) for discharge is based on the following assumptions: To simplify the mathematical description of the heat-transfer phenomena in the complex system shown in Figure 1, the U-tube heat exchanger is positioned axially down the center of the column and approximated as a single tube with the diameter doubled. The outside of the column is assumed to be perfectly insulated, whereas the water temperature inside the heat exchanger is assumed to be constant throughout the discharge process. All heat-transfer processes between the material and the heat exchanger are lumped together and described by an overall heat-transfer coefficient. The heat transfer is assumed to occur between the solid mixture and the outside walls of the heat-exchanger tube, which is held at a constant temperature equal to the water temperature. The effect of the mass-transfer resistance is accounted for based on a linear driving force (LDF) approximation, which rigorously assumes a solid diffusion mechanism.[22] The discharge process starts from a fully charged state at a constant temperature and pressure. Because the hydrogen flow rate is constant at the discharge end and zero at the closed end, this leads to the assumption that the flux variation inside the column is linear.[2] All radial gradients are also ignored; hence, ideal plug flow is assumed. The H_2 flow rate demand at the outlet (f_o) is also left as an arbitrary user- or system-defined function.

Based on these assumptions and assuming ideal gas behavior, the 1-D mass balance is given by

$$\frac{1}{\theta}\frac{\partial \pi}{\partial \tau} - \frac{\pi}{\theta^2}\frac{\partial \theta}{\partial \tau} + \frac{\partial \omega}{\partial \xi} + \frac{\partial \phi}{\partial \tau} = 0 \quad (17)$$

where ϕ, π, θ, and ω denote dimensionless loading, pressure, temperature, and molar flux, respectively. The corresponding energy balance, including compression, is written as

$$\left[1 + k_a \frac{\theta}{\pi}\right]\frac{\partial \theta}{\partial \tau} + k_c \frac{\theta}{\pi}\frac{\partial \phi}{\partial \tau} - k_b \frac{\theta}{\pi}\frac{\partial \pi}{\partial \tau} + \frac{\omega\theta}{\pi}\frac{\partial \theta}{\partial \xi} + k_h(\theta - \theta_W) = 0 \quad (18)$$

where k_a, k_b, k_c, and k_h are defined as

$$k_a = \frac{C_{ps}}{q_0 C_{pg}}; \quad k_b = \frac{R}{C_{pg}}; \quad k_c = \frac{\Delta H}{C_{pg} T_0};$$

$$k_h = \frac{2hr_i t_0 RT_0}{\epsilon_2(r_o^2 - r_i^2)C_{pg}P_0 M_{H_2}}$$

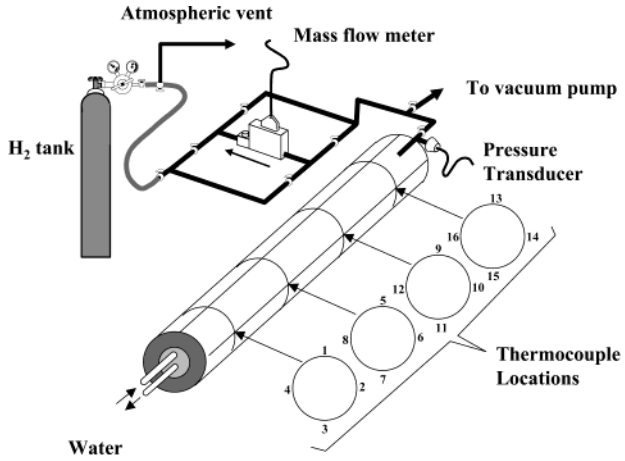

Figure 2. Schematic of the metal hydride hydrogen storage test facility: thermocouples 1, 5, 9, and 13 (top, 355°); thermocouples 2, 6, 10, and 14 (RHS, 95°); thermocouples 3, 7, 11, and 15 (bottom, 191°); thermocouples 4, 8, 12, and 16 (LHS, 260°).

The intraparticle mass-transfer mechanism is based on the following LDF expression:

$$\frac{d\phi}{d\tau} = k_m(\phi^* - \phi) \tag{19}$$

where k_m is the mass-transfer coefficient and ϕ^*, the dimensionless equilibrium loading, is obtained directly from the isotherm relationship.

To solve this system of equations, first, the rate of discharge f is specified as a flow rate at STP. The remaining unknowns are the heat- and mass-transfer coefficients, h and k_m. They are obtained by fitting the pressure and temperature histories obtained from the model during discharge to the experimental ones, as explained in more detail later. With h and k_m specified, eqs 17−19, along with a suitable $P-C-T$ relationship, can be input to FEMLAB and solved simultaneously with the following initial conditions: at $t = 0$, $\pi = \pi_i$, $\theta = \theta_i$, and $\phi = \phi_i$ (obtained from the isotherm at π_i and θ_i). Again, it is a simple matter to convert this model into one that describes the charge process by changing the initial conditions.

Experimental Section

A schematic of the hydrogen storage test facility containing $Lm_{1.06}Ni_{4.96}Al_{0.04}$ metal hydride is shown in Figure 2. The SRTC column is equipped with 16 K-type thermocouples mounted externally on the stainless steel surface at four axial locations, with each axial location having four thermocouples set approximately 90° apart from each other (95°, right-hand side (RHS); 191°, bottom; 260°, left-hand side (LHS); 355°, top). Standard pipe insulation with a wall thickness of 0.075 m is placed around the column to insulate the external surface from ambient temperature variations. A thermocouple is also mounted on the external surface of the insulation to monitor the changes in the ambient temperature. Thermocouples are positioned inline at the inlet and outlet of the U-tube heat exchanger and the inlet/outlet of the hydrogen feed tube. The water flow rate through the heat exchanger is maintained constant at 5 gpm, which ensures less than a 0.5 °C temperature differential between the inlet and outlet temperatures of the heat exchanger. The heat-exchanger water temperature is relatively constant at 29 °C. The pressure inside the column is measured just at the outlet of the column using an Omega PX303-500G5V (with an accuracy of 0.25% full scale) pressure transducer, and the hydrogen discharge flow rate is controlled with a Hastings MFC 203 mass flow controller (with an accuracy of ±1% of full scale). The Labview-based data acquisition system (DAS) records all of the temperatures, the pressure, and the hydrogen and water flow rates. The HP-grade H_2 (99.99% purity), supplied by National Welders, is used as received.

A typical discharge run is carried out as follows. The bed is filled with hydrogen at 100 SLPM through the mass flow controller to the desired pressure (∼25 atm). The bed is allowed to cool and equilibrate at the desired pressure until all of the temperatures level off at the ambient condition. Then the bed is discharged at a constant molar flow rate (5−40 SLPM), and the pressure and temperatures are recorded using the DAS. Each run ends when the desired molar flow rate is no longer sustainable.

Results and Discussion

Six hydrogen discharge experiments were carried out at 5, 10, 15, 20, 25, and 40 SLPM hydrogen demand in the metal hydride hydrogen storage test facility. The resulting pressure discharge histories are shown in Figure 3a. As the molar flow rate demand increased, the time that the column could sustain the desired flow rate also decreased, especially at the higher flow rates. For example, at 5, 10, 15, 20, 25, and 40 SLPM the system could no longer sustain the flow rate after 12, 6, 4, 3, 2.5, and 1.5 h of discharge, respectively. Figure 3b illustrates the typical temperature histories obtained at the different thermocouple locations for the 20 SLPM hydrogen flow rate run. Notice that the external surface of the insulation, the ambient temperature, hydrogen discharge temperature, and heat-exchanger water inlet and outlet temperatures were nearly constant, with each varying less than 0.2 °C during the run and all being around 23 °C. The water outlet temperature was consistently about 0.5 °C cooler than the inlet temperature, indicating that water was transferring some energy to the metal hydride bed. The temperatures at the same angular position, but at different axial positions, also nearly overlapped with each other. This indicated that the metal hydride was placed uniformly in the axial direction and, more importantly, from a modeling point of view that axial gradients were negligible. In contrast, significant angular temperature gradients were observed that were different at each angular location, but consistent with the vessel being only three-quarters filled with metal hydride to allow for expansion, as shown in Figure 1. These angular gradients may have also been due to the variation in the placement of the thermocouples around the vessel because the thermocouples were not exactly at 0°, 90°, 180°, and 270°, as indicated.

The bottom four thermocouples running along the axis (at ∼191° from the top center) exhibited the least drop in temperature, followed by those on the top of the column (∼355°), then the LHS (∼260°), and finally the RHS (∼95°). Those positioned along the bottom are the closest to the bottom rung of the U-tube heat exchanger, which also happens to be the inlet tube. The effect of the 5 gpm, 29 °C water as a source of energy input to the system was obvious. Those positioned along the top exhibited a substantial decrease in temperature most

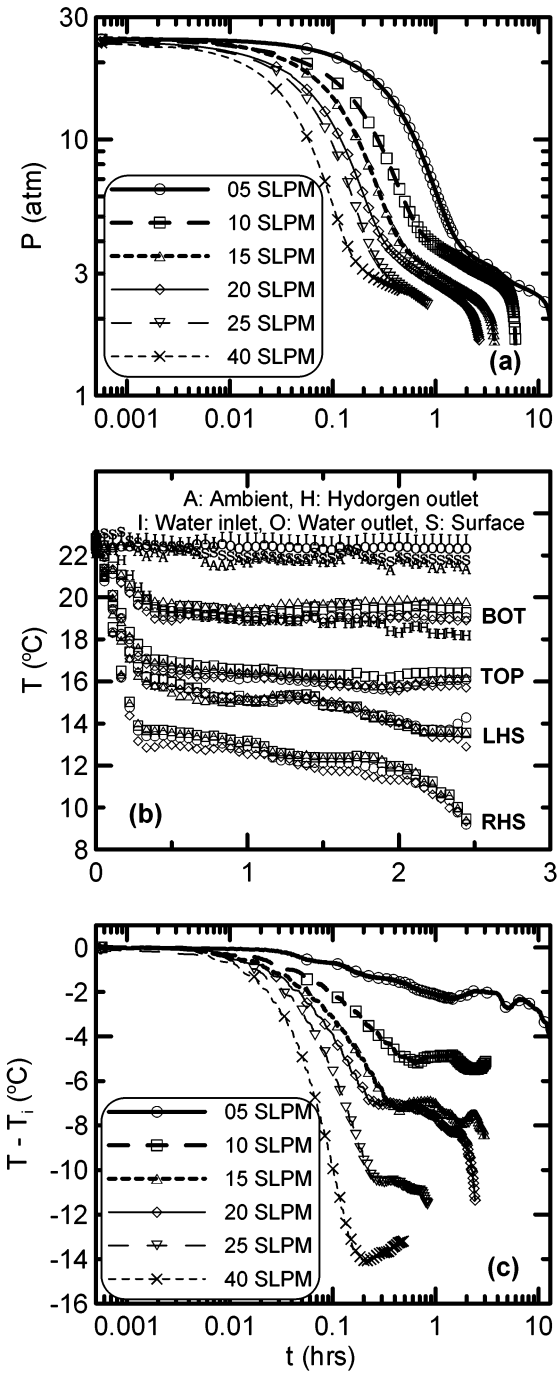

Figure 3. (a) Experimental pressure histories during discharge for each of the six hydrogen flow-rate demands. (b) Typical temperature histories obtained at the different thermocouple locations (refer to Figure 2) during discharge for each of the six hydrogen flow-rate demands. (c) Average axial temperature variation (in terms of the deviation from the initial bed temperature) on the RHS (91°) of the metal hydride vessel during discharge for each of the six hydrogen flow-rate demands.

likely because they were located the farthest away from either of the two heat-exchanger tubes. This was not the greatest decrease in temperature, however, because the top 25% of the column did not contain any metal hydride. The LHS and RHS of the column both exhibited slightly greater decreases in temperature because this is where the metal hydride was located and they were farther away from the heat-exchanger tubes compared to the bottom. Ideally, the LHS and RHS temperatures should be the same if the metal hydride is distributed evenly throughout the aluminum foam and if the thermocouples are positioned exactly at 90° and 270°, which they were not. Either one of these conditions could have caused the RHS to be 3 °C cooler than the LHS.

Similar trends were observed with the other five runs, but with more marked decreases in temperature as the flow rate demand increased. This effect is shown in Figure 3c, which displays the average axial temperature variation (deviation from the initial bed temperature) on the RHS of the metal hydride bed during discharge at the six different constant molar flow rates. The higher hydrogen flow rate demands clearly corresponded to faster discharge times down to the pressure plateau regions, as expected, when starting from essentially the same initial conditions in all runs. However, higher hydrogen demands also consistently corresponded to lower pressure plateaus. This last result was a consequence of the shift in the plateau region on the adsorption isotherm to lower pressures with a decrease in temperature. The pressure and temperature histories, in all cases, showed an initial rapid drop during discharge and then essentially leveled off during the remainder of the experiment. These interesting plateaus are associated with the phase-change region of the $P-C-T$ diagram, which is clearly visible in Figure 4a for the $Lm_{1.06}Ni_{4.96}Al_{0.04}$ metal hydride hydrogen system.

To model the experimental discharge results, the experimental $P-C-T$ data for the $Lm_{1.06}Ni_{4.96}Al_{0.04}$ metal hydride system (provided by the SRTC[21]) were fitted to both the CL and MV models using nonlinear regression. The results are also shown in Figure 4a, and the corresponding parameters are given in Table 1. The two experimental isotherms at 313 and 333 K and the numerous $P-T$ data points at constant loading above and below the phase transition region were correlated equally well by both models. The corresponding heats of adsorption predicted by the two models are shown in Figure 4b. Both models predicted reasonably similar and relatively constant values in the phase-change region: 28 and 33 kJ/mol for the CL and MV models, respectively. The predicted behaviors outside the phase transition region were fundamentally different, however. The MV model exhibits convex behavior and the CL model exhibits concave behavior relative to the abscissa; the CL model also predicts a slight temperature dependence, whereas the MV formulation predicts a temperature-independent heat of adsorption. Nevertheless, because the fits of these models to the experimental data were both very good, either of these relationships could be used to predict the hydrogen loading as a function of temperature and pressure over a wide range of conditions. The effect of these different $P-C-T$ formulations becomes more evident upon predicting the dynamic discharge behavior, as shown later.

In addition to the $P-C-T$ model parameters, the heat- and mass-transfer coefficients were also needed to model the experimental discharge results. Of the six hydrogen discharge experiments carried out at 5, 10, 15, 20, 25, and 40 SLPM hydrogen demand, one of them was chosen arbitrarily (the 20 SLPM run) to calibrate the NM by varying h and k_m until the pressure and temperature histories from the model approximately matched the experimental data, based on visual inspection. The performances of the other five runs were predicted using these coefficients without further adjustment. The heat- and mass-transfer coefficients

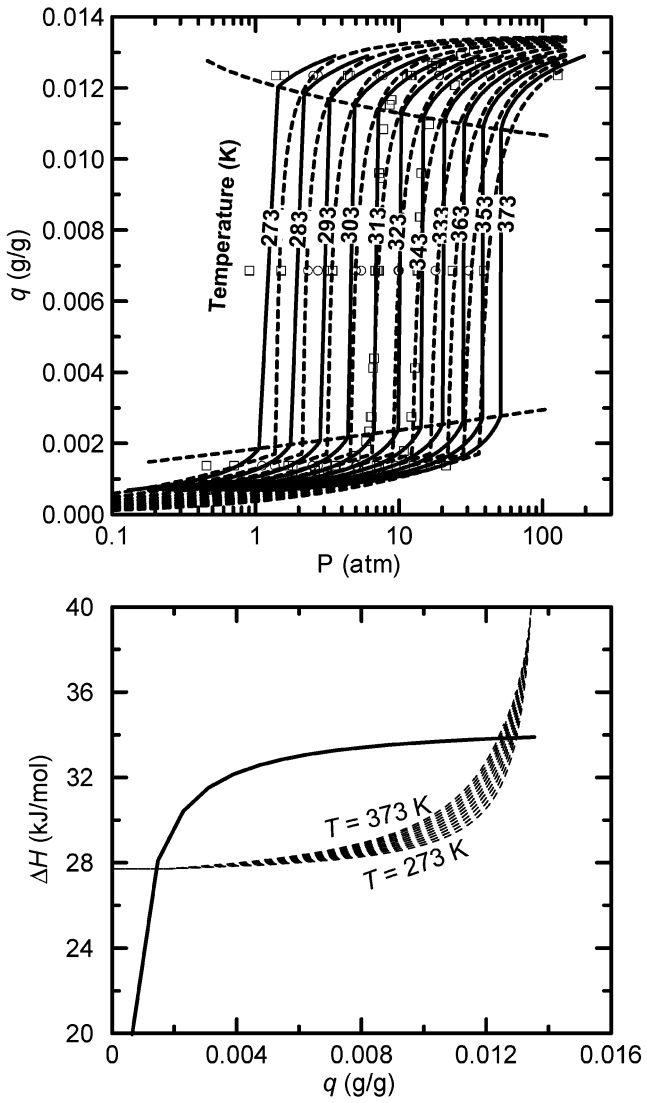

Figure 4. (a) $Lm_{1.06}Ni_{4.96}Al_{0.04}$ metal hydride hydrogen isotherms (symbols, experiment; solid lines, MV correlation; dashed lines, CL correlation). (b) Isosteric heat of adsorption (solid lines, MV correlation; dashed lines, CL correlation).

Table 1. *P*−*C*−*T* Parameters

	MV Isotherm		
A_0	22.0628	a_H	525 528.8838
A_1	−15.2353	b_H	343 762.133
B_0	−576.1705	a_L	20.3901
B_1	320.1486	b_L	−10.0091
C_0	7.8109×10^{-40}		
	CL Isotherm		
ϕ_S	130.4753	b_{20} (atm$^{-0.5}$)	0.002 506 4
d_0	24.053	ΔH_1 (kJ kg^{-1})	−6.9285
ϕ_{max}	1028.1644	ΔH_2 (kJ kg^{-1})	−10.3270
b_{10} (atm$^{-0.5}$)	0.000 751 2	ΔH_S (kJ kg^{-1})	−13.8575

obtained from the MV model were $h = 1.3 \times 10^{-2}$ W/cm^2/K and $k_m = 0.1$, and those from the CL model were 7.6×10^{-3} W/cm^2/K and $k_m = 0.1$. These values were uniquely defined in each case, with both models resulting in the same k_m and nearly the same h. The fact that the same dimensionless value of k_m was obtained for all of the discharge flow rates suggested that the dimensional value of the mass-transfer coefficient (k_L) was directly proportional to the discharge flow rate. However, k_L turned out to be a weak function of flow rate, most likely because in all cases near

Table 2. Model Parameters and Operating Conditions

r_o (m)	0.045
r_i (m)	0.02
L (m)	1.52
m_{mH} (kg)	26.078
m_{Al} (kg)	1.789
ρ_{mH} (kg/m^3)	8700
ρ_{Al} (kg/m^3)	2700
f_r	0.702
ϵ_{mH}	0.4
ϵ_{Al}	0.915
C_{pg} (kJ/kg/K)	14.42
C_{ps} (kJ/kg/K)	0.419
H_2 discharge flow rate (SLPM)	5−40
T (ambient) (K)	292−295
T_i (K)	292−295
P_i (atm)	∼25
k_m	0.1
h (MV isotherm) (W/cm^2/K)	1.3×10^{-2}
h (CL isotherm) (W/cm^2/K)	7.6×10^{-3}

equilibrium conditions prevailed as indicated by the mass-transfer driving force always being very small (i.e., $\phi^* - \phi \sim 0$ in eq 17). It was also observed that the model predictions were very sensitive to the magnitude of the heat-transfer coefficient, possibly indicating that the discharge process was heat-transfer-limited, similar to that reported elsewhere for metal hydride beds.[23] The factor of 2 difference in the h's from the MV and CL models was most likely caused by the difference in the plateau heat of adsorption for the two $P-C-T$ models. The CL model had the lower heat of adsorption (by 5 kJ/mol), and this was consistent with the CL model also resulting in a smaller value of h. Table 2 lists all of the parameters that were used in the model simulations.

The experimental pressure histories obtained during discharge for all six runs are shown in Figure 5, along with model predictions from both the CL and MV models using the fitted values of h and k_m (Non Ad, Non Eq). The corresponding temperature histories are shown in Figure 6. Note that each experimental temperature history corresponds to the average temperature associated with all 16 thermocouples. The pressure and temperature predictions from the nonadiabatic nonequilibrium models utilizing the two different $P-C-T$ relationships (CL and MV) were quite satisfactory and similar; however, the one based on the MV model gave slightly better results, especially for the temperature histories of the 20 and 40 SLPM runs. For this reason, the MV model was chosen to show the extreme behaviors, under isothermal equilibrium conditions (Iso, Eq) with $h = k_m = \infty$, adiabatic equilibrium conditions (Ad, Eq) with $h = 0$ and $k_m = \infty$, and adiabatic nonequilibrium conditions (Ad, Non Eq) with $h = 0$ and $k_m = k_m$ (fitted); these results are also plotted in Figures 5 and 6. The two additional cases not shown in these figures, i.e., nonadiabatic equilibrium (Non Ad, Eq) with $h = h$ (fitted) and $k_m = \infty$ and isothermal nonequilibrium (Iso, Non Eq) with $h = \infty$ and $k_m = k_m$ (fitted) essentially overlapped the nonadiabatic nonequilibrium (Non Ad, Non Eq) and isothermal equilibrium (Iso, Eq) profiles, respectively. The fact that the nonadiabatic equilibrium predictions always overlapped in all cases with the nonadiabatic nonequilibrium predictions further substantiated that the SRTC system operated essentially without any mass-transfer limitations but was definitely heat-transfer-limited. Nevertheless, in all cases, the adiabatic predictions deviated markedly from the experimental results, indicating that the heat-exchanger water flow rate was sufficient enough to allow the

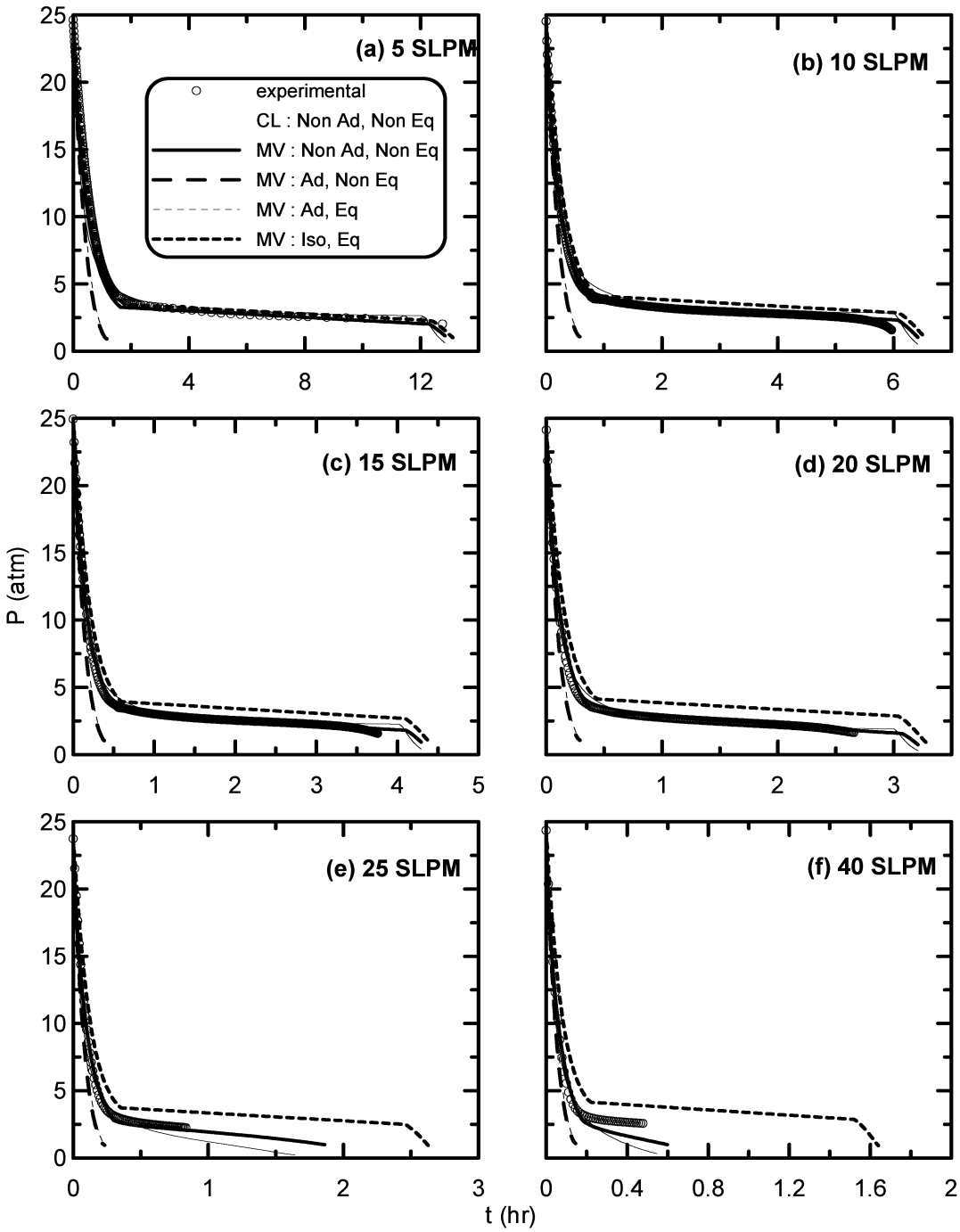

Figure 5. Comparison of various model predictions with the experimental pressure histories for the six hydrogen flow-rate demands: CL, composite Langmuir; MV, modified virial; Non Ad, nonadiabatic; Non Eq, nonequilibrium; Ad, adiabatic; Eq, equilibrium; Iso, isothermal. Note that the profiles obtained from the Non Ad, Eq and Iso, Non Eq models (not shown) completely overlapped those from the Non Ad, Non Eq and Iso, Eq models, respectively.

system to operate nearer to isothermal conditions. In fact, the isothermal equilibrium conditions prevailed at the lower flow rate of 5 SLPM, as indicated by the excellent agreement between the isothermal equilibrium model and the experimental discharge profiles. This result validated the use of the CL and MV $P-C-T$ models for predicting the equilibrium characteristics of the $Lm_{1.06}Ni_{4.96}Al_{0.04}$ metal hydride. However, at the higher flow rates, although the pressure histories were predicted quite well by the two models using the fitted values of h and k_m, i.e., the most realistic models, these two nonadiabatic nonequilibrium models failed to predict the leveling off of the temperature history of the 40 SLPM run. This indicated that the overall heat-transfer approach was not quite rigorous enough to capture the behavior of the SRTC vessel at high hydrogen flow rates; hence, more rigorous models are under development.

As stated above, the same set of heat- and mass-transfer coefficients was able to predict the experimental discharge profiles with reasonable accuracy for the given isotherm, and because the set of governing equations were solved in dimensionless form, the only quantities varying for the different operating conditions (various hydrogen flow rates) were the initial conditions and outside temperature. Thus, when the same set of equations was solved for the adiabatic condition, they became identical in dimensionless form, except for the

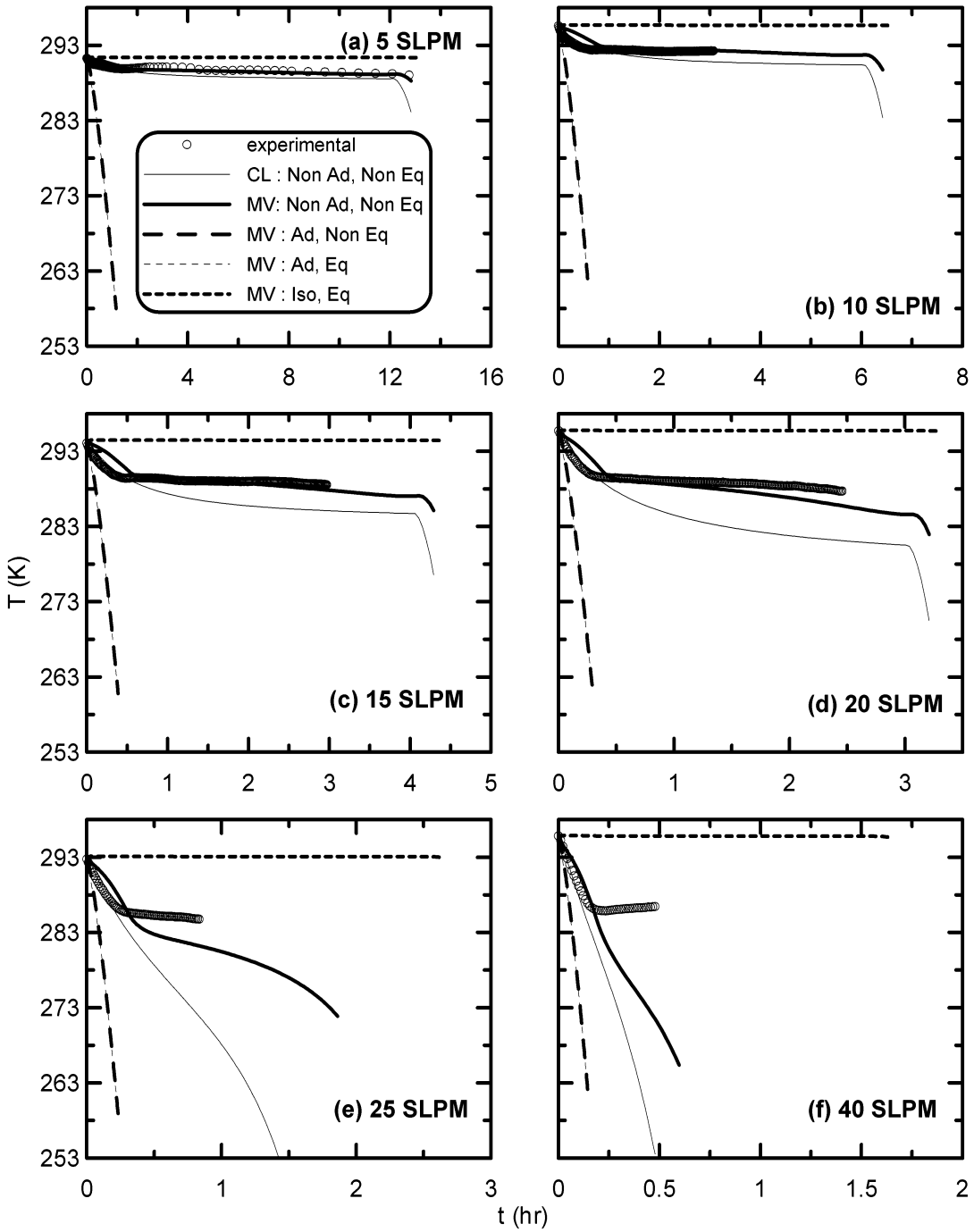

Figure 6. Comparison of various model predictions with the experimental temperature histories (average of all 16 thermocouples; see Figure 2) for the six hydrogen flow-rate demands: CL, composite Langmuir; MV, modified virial; Non Ad, nonadiabatic; Non Eq, nonequilibrium; Ad, adiabatic; Eq, equilibrium; Iso, isothermal. Note that the profiles obtained from the Non Ad, Eq and Iso, Non Eq models (not shown) completely overlapped those from the Non Ad, Non Eq and Iso, Eq models, respectively.

time constants and the initial conditions. If the corresponding pressure and temperature histories are plotted on the same graph, they would be proportional to each other, with the proportionality factor being the time constant for each case. By extension of this analysis to the nonadiabatic simulations, if the outside temperatures are within close proximity to each other for each individual case, the discharge times predicted by the nonadiabatic models should again be inversely proportional to the hydrogen flow rate demand, which was indeed the case. For example, the 5 SLPM run took nearly 12 h for the pressure to discharge (Non Ad, Non Eq). In contrast, it takes just about half that time, i.e., 6 h for the 10 SLPM run, 4 h for the 15 SLPM run, 3 h for the 20 SLPM run, and 2.5 h for the 25 SLPM run. However, for the 40 SLPM, because the simulation was stopped when the pressure reached 1 atm, it was not possible to observe this proportional behavior.

Another interesting observation pertained to the simulated isothermal equilibrium discharge. The pressure discharge histories predicted from this model compared very well with the experimental results at the lower flow rates and then began to deviate from the experimental data with increasing hydrogen flow rate demand. This was expected because mass-transfer limitations were always minimal and the total temperature variation during the discharge process was always less at the lower flow rates. Certainly, however, the 5

gpm, 29 °C heat-exchanger water had a substantial influence on the heat-transfer characteristics of this system. Nevertheless, according to the model, the isothermal equilibrium discharge represents the upper thermodynamic limit and therefore represents the best possible performance. One of the goals during design considerations is to achieve this performance because it extends the duration for which this unit could keep on supplying hydrogen at the desired flow rate. This means that better heat-transfer characteristics have to be achieved to improve the performance of a metal hydride hydrogen storage unit. To this end, the SRTC metal hydride vessel uses aluminum foam for improved internal heat conduction and the heat exchanger for heat transfer, as shown in Figure 1. Whether this is the most optimum design has yet to be determined; a detailed study is underway.

Conclusions

Mathematical models of varying complexity, ranging from isothermal equilibrium to isothermal nonequilibrium to adiabatic equilibrium to nonadiabatic equilibrium to adiabatic nonequilibrium to nonadiabatic nonequilibrium conditions, were developed to predict the discharge performance of a commercially viable metal hydride hydrogen storage vessel containing $Lm_{1.06}Ni_{4.96}Al_{0.04}$. Two new semiempirical $P-C-T$ models, one based on a MV isotherm relationship and the other based on a CL isotherm relationship, were also introduced and used within the models to predict the equilibrium behavior in lieu of the typical empirical van't Hoff $P-C-T$ relationship. Also, the typical reversible reaction kinetic mechanism was replaced with a solid diffusion mechanism, which is a new approach in the modeling of metal hydride hydrogen storage vessels.

The predictive ability of these models was contrasted against six experimental discharge runs obtained over a wide range of hydrogen flow rate demands (5−40 SLPM). Under isothermal equilibrium conditions, an analytical solution was obtained for the discharge performance, which represented the upper thermodynamic limit and hence the best possible performance. For the experimental conditions, which in all cases included heat exchange within the vessel using 29 °C water flowing at 5 gpm through a U-tube heat exchanger, the run carried out at the 5 SLPM hydrogen flow rate demand compared very well with the isothermal equilibrium model. This result validated the use of the CL and MV $P-C-T$ models for predicting the equilibrium characteristics of the $Lm_{1.06}Ni_{4.96}Al_{0.04}$ metal hydride. The other runs at the higher flow rates, as expected, did not agree with the isothermal equilibrium model and required a more realistic approach to predict the performance. The remaining models required a numerical solution because they realistically accounted for heat- and mass-transfer resistances.

The nonadiabatic nonequilibrium model, the most realistic model, was used to determine the heat- and mass-transfer coefficients that characterized the experimental system by fitting the model to one of the experimental discharge experiments (arbitrarily selected). The same dimensionless mass-transfer coefficient ($k_m = 0.1$) and nearly the same heat-transfer coefficients (7.6×10^{-3} versus 1.3×10^{-2} W/cm^2/K) were obtained when using either the CL or MV isotherm models, respectively. These results gave some credence to the assumed heat- and mass-transfer mechanisms. Overall, the results showed that a fairly simple NM could do a reasonable job in predicting the discharge behavior (i.e., the pressure and temperature histories) of a fairly complicated metal hydride hydrogen storage bed over a wide range of hydrogen demands. However, the MV model did perform slightly better than the CL model in predicting the pressure and temperature histories; therefore, it was used to model the behavior of the system under extreme, limiting conditions.

These limiting cases revealed that the metal hydride hydrogen storage vessel was definitely heat-transfer-limited and only minimally mass-transfer-limited over a wide range of hydrogen discharge flow rates. Also, in all cases, the adiabatic predictions deviated markedly from the experimental results, indicating that the internal heat-exchanger water flow rate (5 gpm) and temperature (∼29 °C) were sufficient enough to allow the system to operate nearer to isothermal conditions. However, although the pressure histories were predicted very well in all cases, the nonadiabatic nonequilibrium model failed to predict the temperature history of the 40 SLPM run. This indicated that a more rigorous approach than the use of an overall heat-transfer mechanism needs to be considered. For this reason, more sophisticated models are being developed that will eventually lead to better designs of metal hydride hydrogen storage vessels.

Acknowledgment

Financial support provided by the National Reconnaissance Office under Contract No. NRO-00-C-0134 is greatly appreciated. The metal hydride hydrogen storage vessel and the metal hydride $P-C-T$ data provided by the Hydrogen Technology Section of the Savannah River Technology Center are also greatly appreciated.

Nomenclature

c = gas-phase hydrogen concentration (kg/m^3)
C_{ps} = specific heat of the solid (kJ/kg/K)
C_{pg} = specific heat of the gas (kJ/kg/K)
d_0 = bed diameter (m)
f = molar flux (mol/cm^2/s)
f_0 = standard flux (mol/cm^2/s)
f_r = fraction of aluminum voids filled with metal hydride particles with packing porosity ϵ_{mH}
h = heat-transfer coefficient (W/cm^2/K)
ΔH = isosteric heat of adsorption (kJ/kg/K)
k = velocity gradient in the bed (v_{out}/L)
k_L = LDF mass-transfer coefficient (s^{-1})
k_m = dimensionless mass-transfer coefficient used in the simulation ($k_L t_0$)
L = bed length (m)
M_{H_2} = molecular weight of hydrogen (g/mol)
m_{mH} = mass of metal hydride (kg)
m_{Al} = mass of aluminum (kg)
P_i = initial pressure (atm)
P_0 = standard pressure (1 atm)
q = hydrogen loading (kg/kg)
q_i = initial hydrogen loading (kg/kg)
q_0 = standard hydrogen loading ($\epsilon_2 P_0/(1-\epsilon_1)\rho_{mH} R T_0$)
r_o = outside radius of the vessel (m)
r_i = radius of the coaxial heat-exchanger tube (m)
R = gas law constant (m^3·atm/kmol·K)
t = discharge time (s)
T = temperature (K)
T_i = initial temperature (K)
T_0 = standard temperature (273.15 K)

t_0 = time constant ($\epsilon_2 P_0 L/RT_0 f_0$) (s)
v = gas-phase velocity (m/s)
v_{out} = constant outlet velocity (m/s)
z = axial distance inside the bed (m)

Greek Letters

π = dimensionless pressure (P/P_0)
θ = dimensionless temperature (T/T_0)
ϕ = dimensionless hydrogen loading (q/q_0)
ϕ^* = dimensionless equilibrium loading (q^*/q_0)
ρ_{mH} = metal hydride density (kg/m^3)
ρ_{Al} = aluminum skeleton density (kg/m^3)
ϵ_1 = volume fraction of bed not occupied by metal hydride particles
ϵ_2 = volume fraction of bed not occupied by either metal hydride particles or aluminum foam
ϵ_{Al} = volume fraction of pores in aluminum foam
ϵ_{mH} = volume fraction of interstitial voids between packed metal hydride particles
τ = dimensionless time (t/t_0)
ω = dimensionless molar flux demand (f/f_0)

Literature Cited

(1) Heung, L. K. On-board Hydrogen Storage System Using Metal Hydride. *HYPOTHESIS II* **1997**, 1.

(2) Lamari, M.; Aoufi, A.; Malbrunot, P. Thermal Effects in Dynamic Storage of Hydrogen by Adsorption. *AIChE J.* **2000**, *46*, 632.

(3) Mat, M. D.; Kaplan, Y. Numerical Study of Hydrogen Absorption in an Lm-Ni_5 Hydride Reactor. *Int. J. Hydrogen Energy* **2001**, *26*, 957.

(4) Levesque, S.; Ciureanu, M.; Roberge, R.; Motyka, T. Hydrogen Storage for Fuel Cell Systems with Stationary Applications—I. Transient Measurement Technique for Packed Bed Evaluation. *Int. J. Hydrogen Energy* **2000**, *25*, 1095.

(5) Klein, J. E.; Brenner, J. R.; Dye, E. F. Development of a Passively Cooled, Electrically Heated (PACE) Bed. *Fusion Technol.* **2002**, *41*, 782.

(6) Das, L. M. On-board Hydrogen Storage Systems for Automotive Application. *Int. J. Hydrogen Energy* **1996**, *21*, 789.

(7) Berry, G. D.; Aceves, S. M. On-board Storage Alternatives for Hydrogen Vehicles. *Energy Fuels* **1998**, *12*, 49.

(8) Mungole, M. N.; Balasubramaniam, R. Effect of Hydrogen Cycling on the Hydrogen Storage Properties of $MmNi_{4.2}Al_{0.8}$. *Int. J. Hydrogen Energy* **2000**, *25*, 55.

(9) Gopal, M. R.; Murthy, S. S. Parametric Studies on Heat and Mass Transfer in Metal Hydride Beds. *Chem. Eng. Proc.* **1993**, *32*, 217.

(10) Sun, D.; Deng, S. Study of the Heat and Mass Transfer Characteristics of Metal Hydride Beds. *J. Less-Common Met.* **1988**, *141*, 37.

(11) Jemni, A.; Nasrallah, S. B.; Lamloumi, J. Experimental and Theoretical Study of a Metal−Hydrogen Reactor. *Int. J. Hydrogen Energy* **1999**, *24*, 631.

(12) Nakagwa, T.; Inomata, A.; Aoki, H.; Miura, T. Numerical Analysis of Heat and Mass Transfer Characteristics in the Metal Hydride Bed. *Int. J. Hydrogen Energy* **2000**, *25*, 339.

(13) Guo, Z. Enhancement of Heat and Mass Transfer in Metal Hydride Beds with the Addition of Al Plates. *Heat Mass Transfer* **1999**, *34*, 517.

(14) Gopal, M. R.; Murthy, S. S. Studies on Heat and Mass Transfer in Metal Hydride Beds. *Int. J. Hydrogen Energy* **1995**, *20*, 911.

(15) Jemni, A.; Nasrallah, S. B. Study of Two-Dimensional Heat and Mass Transfer During Desorption in a Metal−Hydrogen Reactor. *Int. J. Hydrogen Energy* **1995**, *20*, 881.

(16) Jemni, A.; Nasrallah, S. B. Heat and Mass Transfer Models in Metal−Hydrogen Reactor. *Int. J. Hydrogen Energy* **1997**, *22*, 67.

(17) Isselhorst, A. Heat and Mass Transfer in Coupled Hydride Reaction Beds. *J. Alloys Compds.* **1995**, 871.

(18) Valenzuela, D. P.; Myers, A. L. *Adsorption Equilibrium Data Handbook*; Prentice Hall: Englewood Cliffs, NJ, 1989.

(19) Ritter, J. A.; Yang, R. T. Equilibrium Theory for Hysteresis Dependent Fixed Bed Desorption. *Chem. Eng. Sci.* **1990**, *46*, 563.

(20) Mueller, W.; Blackledge, J. P.; Libowitz, G. G. *Metal Hydrides*; Academic Press: New York, 1968.

(21) Savannah River Technology Center, Aiken, SC, unpublished data, 2002.

(22) Liaw, C. H.; Wang, J. S. P.; Greenkorn, R. H.; Chao, K. C. Kinetics of Fixed-Bed Adsorption: A New Solution. *AIChE J.* **1979**, *54*, 376.

(23) Fleming, W. H.; Khan, J. A.; Rhodes, C. A. Effective Heat Transfer in a Metal-Hydride-Based Hydrogen Separation Process. *Int. J. Hydrogen Energy* **2001**, *26*, 711.

Received for review October 31, 2002
Revised manuscript received February 6, 2003
Accepted February 11, 2003

IE020839I